An in situ thermo-mechanical rig for lattice strain measurement during creep using neutron diffraction

Y. Q. Wang, S. Kabra, S. Y. Zhang, C. E. Truman, and D. J. Smith

Citation: Review of Scientific Instruments **89**, 055110 (2018); doi: 10.1063/1.5001085
View online: https://doi.org/10.1063/1.5001085
View Table of Contents: http://aip.scitation.org/toc/rsi/89/5
Published by the American Institute of Physics

An *in situ* thermo-mechanical rig for lattice strain measurement during creep using neutron diffraction

Y. Q. Wang,[1,2,a)] S. Kabra,[3] S. Y. Zhang,[3,4] C. E. Truman,[1] and D. J. Smith[1]
[1]*Department of Mechanical Engineering, University of Bristol, Bristol BS8 1TR, United Kingdom*
[2]*United Kingdom Atomic Energy Authority, Culham Science Centre, Abingdon, Oxfordshire OX13 3DB, United Kingdom*
[3]*ISIS Neutron Facility, RAL, STFC, Didcot, Oxfordshire OX11 0QX, United Kingdom*
[4]*Centre of Excellence for Advanced Materials, Songshan Lake, Dongguan, Guangdong 523808, China*

(Received 21 August 2017; accepted 22 April 2018; published online 18 May 2018)

A long-term high-temperature testing stress rig has been designed and fabricated for performing *in situ* neutron diffraction tests at the ENGIN-X beamline, ISIS facility in the UK. It is capable of subjecting metals to high temperatures up to 800 °C and uniaxial loading under different boundary conditions including constant load, constant strain, and elastic follow-up, each with minimum of external control. Samples are held horizontally between grips and connected to a rigid rig frame, a soft aluminium bar, and a stepper motor with forces up to 20 kN. A new three zone split electrical resistance furnace which generates a stable and uniform heat atmosphere over 200 mm length was used to heat the samples. An 8 mm diameter port at 45° to the centre of the furnace was made in order to allow the neutron beam through the furnace to illuminate the sample. The entire instrument is mounted on the positioner at ENGIN-X and has the potential ability to operate continuously while being moved in and out of the neutron diffraction beam. The performance of the rig has been demonstrated by tracking the evolution of lattice strains in type 316H stainless steel under elastic follow-up control at 550 °C. *Published by AIP Publishing.* https://doi.org/10.1063/1.5001085

I. INTRODUCTION

The concept of elastic follow-up was first introduced by Robinson,[1] as representing a mechanical boundary condition lying between constant load and constant strain control. This mechanical boundary condition can be described by a two-bar model which is a specimen (with stiffness of K_1) connected to a spring (stiffness K_2) in series, as shown in Fig. 1(a), state 1. A locked-in tensile stress can be introduced in the specimen and spring when the two-bar model is subjected to a fixed displacement, δ_0 [Fig. 1(a), state 2]. When the force in the specimen relaxes due to creep, the force/displacement (δ_2) in the spring also relaxes/reduces. The reduced displacement in the spring will then be transferred to the specimen ($\delta_1 = \delta_0 - \delta_2$) as the total misfit ($\delta_0$) is fixed. This displacement redistribution is called the elastic follow-up for creep which can exist in many engineering components operating at high temperature.[2–4]

When the specimen experiences creep while the spring is elastic,[5,6] an elastic follow-up factor, Z, is given by

$$Z = 1 + \frac{1}{\alpha}, \tag{1}$$

where α is the stiffness ratios between the specimen and the spring, given by $\alpha = K_2/K_1$, where $K_1 = A_1E_1/L_1$ and K_2 are the stiffness for the specimen and spring, respectively. A_1, E_1, and L_1 are the cross-sectional area, Young's modulus, and length of the specimen. Unlike under constant load or constant strain control, under elastic follow-up both the stress and total strain in the specimen can change [Fig. 1(b)]. The slope of the stress-strain trajectory during stress relaxation ($\Delta\sigma_1 = \Delta\varepsilon_1$) in Fig. 1(b) represents the value of the elastic[6] follow-up factor (more details can be found in the Appendix).

The presence of elastic follow-up results in a slower stress relaxation rate [Fig. 1(c)] and additional strain accumulation in the specimen [Fig. 1(b)] when compared to a classical stress relaxation test. The result of this is accumulation of creep strain in a localized region, exacerbating problems of crack initiation and fatigue damage. Therefore, predicting the effect of elastic follow-up on creep stress relaxation is important for the structural integrity assessment of high temperature critical plant components. The majority of previous work predicted the stress relaxation and elastic follow-up behavior using a constant-load creep model,[6–14]

$$\dot{\sigma}_1 = -(1/Z)E_1 f_1, \tag{2}$$

where $\dot{\sigma}_1$ is stress rate in the specimen, E_1 is the Young's modulus, and f_1 is a constant-load model derived from constant-load creep data.

However, most recently Wang *et al.*[6,15] showed that Eq. (2) was not able to predict stress relaxation and elastic follow-up using an empirical constant-load model and its constants. This indicated that the boundary conditions could affect the creep deformation mechanisms, such as the change of the evolution of intergranular stress between different grain families. Creep as a time-dependent plastic deformation can generate intergranular strains/stresses in type 316H austenitic stainless steel often during the primary stage of the constant load creep.[16–18] This is due to creep occurring differently along different crystalline planes, thereby creating strain incompatibilities between grain families. The presence of intergranular stress can change the internal resistance and

a)Author to whom correspondence should be addressed: yiqiang.wang@manchester.ac.uk

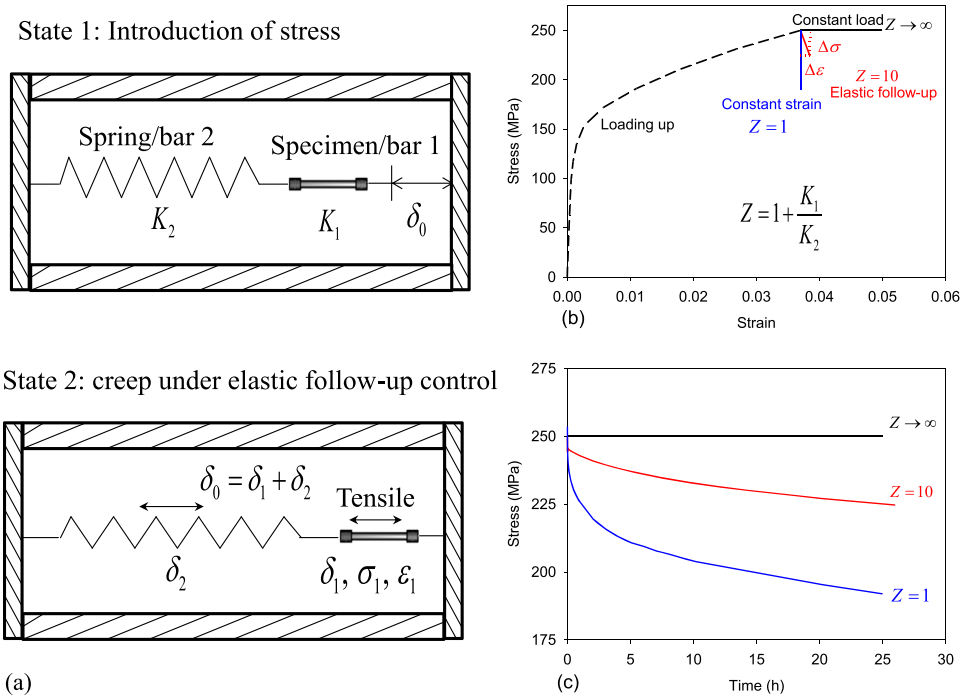

FIG. 1. (a) A two-bar model allows the introduction of a tensile stress and elastic follow-up into the specimen; (b) an example of the stress-strain trajectories for loading up and creep at constant load ($Z \to \infty$), elastic follow-up ($Z = 10$), and constant strain ($Z = 1$) control; (c) the comparison of creep stress relaxation with elastic follow-up factors of infinitely large, 10 and 1.

effective stress in materials which therefore change the material properties.[7,19–21] However, no work has been done to study the effect of elastic follow-up on creep behavior at the grain length scale and along different crystalline orientations. The main reason for this is that elastic follow-up control is not readily achievable using existing sample environments at current neutron facilities. Also in the majority of neutron measurements, the maximum time to conduct an experiment is often limited to a number of days. This is because the stress rigs used in diffraction facilities are confined to servo-hydraulic,[22] servo-electric, or digital control[23,24] test rigs and the heating systems[22,24,25] used on most of these test rigs can only operate for a short duration. However, a key element in examining metals at high temperature is the ability to understand their performance for long durations and this requires using a loading rig that needs minimum intervention during an experiment, especially when using neutron diffraction techniques at high temperature.

The purpose of the rig described in this paper is the ability to perform elastic follow-up tests to understand the evolution of intergranular strains and stresses during forward creep, stress, relaxation, and elastic follow-up. With such an understanding, a new creep model can be developed to predict the stress relaxation and elastic follow-up behavior and account for the elastic follow-up in structural integrity assessments and life extension cases of, for example, the UK's advanced gas-cooled reactors (AGRs). Moreover, it can be operated continuously but also has the ability to be moved into the neutron diffraction beam at selected intervals to obtain intermittent diffraction measurements. In the remainder of the paper, the design of the new stress rig is first described. Then, a set of high-temperature experiments using type 316H stainless steel as test samples is presented to illustrate the capability and performance of the test machine in the ENGIN-X instrument. The key scientific results have been presented in Ref. 26.

II. TEST RIG DESIGN CHARACTERISTICS

The test rig for our neutron diffraction creep experiments under elastic follow-up control was designed to be mounted on the positioner in the ENGIN-X beamline at the ISIS neutron source. A three-dimensional model of the rig frame, extensometry system, loading systems, and integral furnace is shown in Fig. 2. Notably, the design, orientation, and positioning of the furnace proved to be the most critical element in the design of the test machine. The furnace design is described first followed by more details of the remaining elements of the rig frame, specimens, connectors, and finally loading system.

A. Furnace design

There are many different types of furnaces that are suitable for heating test samples and have been used for conducting neutron diffraction measurements.[27,28] These include lamp,[29] current heating, induction, mirror,[29] vanadium,[24] and electrical resistance[30] furnaces. For the experiments proposed in the current study, it was essential that the furnace could be used for long periods (thousands of hours), achieve a stable temperature up to 650 °C for a sample with a 150 mm gauge length, simple to operate and be transported safely with the rig. Most importantly, the furnace must be capable of being in a neutron beamline without compromising neutron diffraction measurements. The electrical resistance furnace is the most widely used in conventional creep tests since it provides a stable and uniform temperature. It is easy to manipulate and can be run without a cooling system and is very durable for long-term tests. These advantages made it suitable for use in the current study but had never been used before in diffraction studies in any neutron beamline. Therefore, a new three-zone split electrical resistance furnace was designed to maximize the neutron diffraction intensity during experiments.

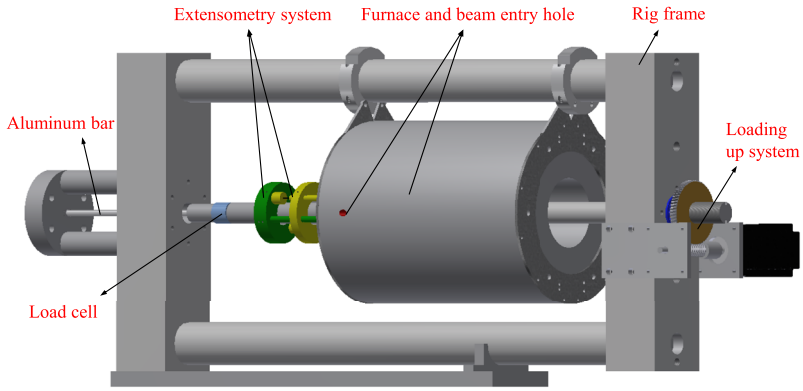

FIG. 2. Three-dimensional model of the rig setup for Z ~ 10.5 including the rig frame, extensometry system, loading up system, integral furnace, load cell, and aluminium bar. The rig frame acts like the rigid frame in a two-bar model, as shown in Fig. 1(a). The aluminium bar represents the spring in Fig. 1(a).

The resistance furnaces are manufactured with a wire wound element for operation on specimens up to 1100 °C.

A cross section of the furnace and its orientation in the ENGIN-X time-of-flight neutron detectors are shown in Fig. 3 (top view). The beamline has two detector banks, centred at 2θ = ±90° to the incident beam. The detectors monitor diffracted neutrons, and within each detector there are five sets of removable radial collimators with distances (L1) of 100, 160, 310, 400, and 490 mm which offer sample gauge volume sizes of 0.5, 1, 2, 3, and 4 mm, respectively.[31] A 4 mm gauge volume was selected in the present study to minimize the measurement time during creep. As the principal interest in the experiments reported in this paper was the axial deformation of test samples, the main axis of the test machine and its furnace had to be orientated at about 45° to the incident beam as shown in Fig. 3. An 8 mm diameter port at 45° to the centre of the furnace was made in order to allow the neutron beam through the furnace to illuminate a sample. Additionally, a 56°, 165 mm long, and 68 mm wide ceramic area was removed to reduce the attenuation of neutrons measured by detector bank 1. The dimensions of the removed area were determined

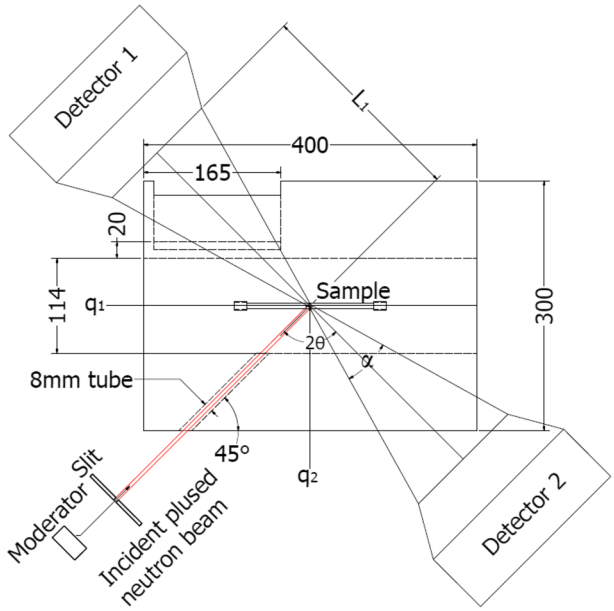

FIG. 3. A schematic plan view of the furnace and its orientation in the ENGIN-X time-of-flight neutron strain scanner. All units are in mm.

according to the coverage of the detector banks which corresponded to ±16° and ±21° in the horizontal and vertical planes, respectively.[31] Except for the 25 mm thick internal furnace insulation wall, no part of the furnace was in the path of the neutron incoming and scattering paths. This provided good quality neutron-diffraction data. The weight, overall length, diameter, and furnace bore diameter of the furnace were 33 kg, 400 mm, 300 mm, and 114 mm, respectively.

A separate unit contained all the equipment necessary for the control of the furnace system and included Eurotherm 3216 temperature controllers for each of the three heating zones. The power supply and furnace controller were operated remotely by using a 15 m cable.

B. Stress rig frame

Based on the constraints of the furnace dimensions and the ENGIN-X test environment, a rigid frame of overall length 1100 mm was manufactured (using EN24T steel), as shown in Figs. 2 and 4. The diameter of the two outside bars was selected to be 70 mm. Two end plates had dimensions of width 120 mm, length 500 mm, and thickness 100 mm. The end plates were designed to place the rig either vertically or horizontally on a table. The length of 520 mm for the end plates was selected in order to accommodate a 300 mm diameter furnace and the two 70 mm diameter outer bars. The thickness of 100 mm ensured that the deflection of each end plate was smaller than 5 μm when applying a force of 20 kN. The test samples and spring/connectors were designed to achieve target values of the elastic follow-up. These are described in Secs. II C and II D.

C. Test sample and connectors for Z ~ 1

The stiffness of the specimen was designed to be as small as possible in order to obtain an elastic follow-up factor close to 1. A 150 mm long specimen with diameter 6 mm was designed to ensure that a neutron diffraction measurement gauge volume of 3 × 3 × 4 mm^3 could easily be accommodated. This gauge volume was selected to provide a measurement time of about 5 min for a single strain measurement in steel. The stiffness of the creep specimen (K_1) was equal to 28.3 kN/mm. Since it was required to achieve Z ~ 1, an additional spring K_2 was not required.

Nevertheless, the connectors and fittings designed to connect the test specimen to the end plates introduced additional

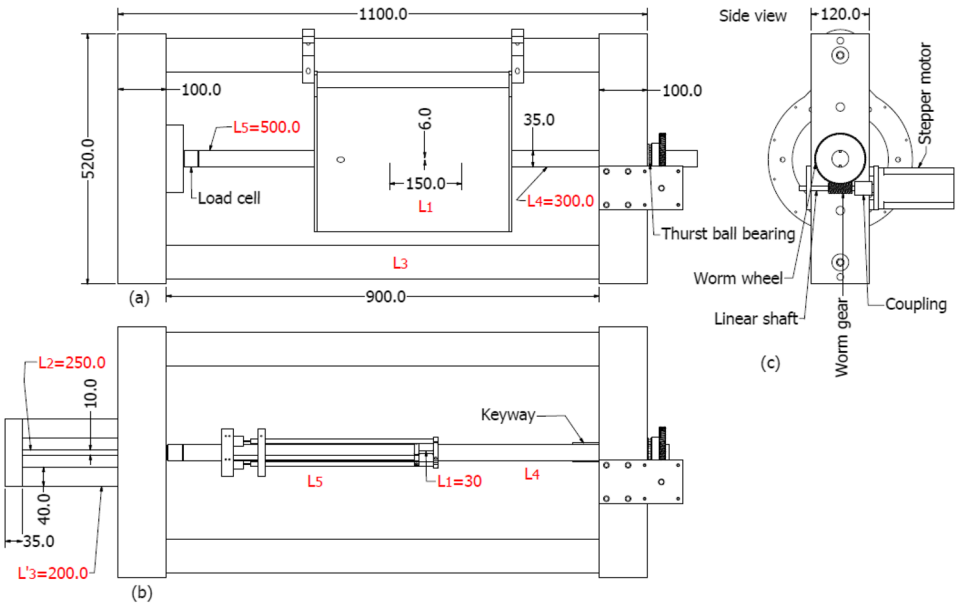

FIG. 4. Schematic drawings of the ENGIN-X rig frame and loading up system; (a) design for Z ~ 1.2 with a 150 mm gauge length and a 6 mm diameter test sample; (b) design for Z ~ 10.5 using a new specimen (length 30 mm, diameter 7 mm) coupled to an aluminium round bar specimen (length 250 mm, diameter 10 mm); (c) the connection of the stepper motor, coupling, linear shaft, worm gear, worm wheel, thrust ball bearing, and keyways.

elastic follow-up. These connectors and fittings, all in series, included a top loading bar (L_4 = 300 mm), an end loading bar (L_5 = 500 mm), two adaptors, a load cell (L_7 = 30 mm), and a load cell end fitting, as shown in Fig. 4(a). Two loading bars were used to connect the creep specimen with adaptors to the load cell and the top plate. Consequently, two adaptors and part of the loading bars were inside the furnace. These parts were manufactured from Nimonic 80A which is a material with good creep resistance properties relative to the test sample. The diameter of the loading bars was selected to be 35 mm. Increasing the diameter of the loading bars increased the stiffness of the rig but decreased the temperature performance of the furnace since larger diameter bars lead to greater thermal losses. The load cell end fitting with diameter 100 mm was made to link the load cell to the end plate. A load cell was screwed in the middle of the disc, and the disc was fixed to the end bottom plate.

On the basis of the various dimensions of the fittings and connectors, the elastic follow-up was determined using

$$Z = 1 + \frac{1}{a} = 1 + \frac{K_1}{K_{CF}}, \tag{3}$$

where K_{CF} represents the total stiffness of the connectors and fittings (CF). These connectors and fittings acted like multiple springs and hence introduced elastic follow-up into the specimen during creep stress relaxation. The designed dimensions of these connectors and fittings resulted in K_{CF} = 254 kN/mm. The final elastic follow-up factor was determined using Eq. (3) and found to be 1.2 which was very close to the target value of about 1. The extra 0.2 elastic follow-up has very minimum effect on the creep stress relaxation.[6]

D. Test sample and connectors for Z ~ 10.5

A larger elastic follow-up factor (Z ~ 10.5) was obtained by using a short specimen with 30 mm length and diameter 7 mm (stiffness K_1 = 192 kN/mm) connected in series to a 250 mm length, 10 mm diameter aluminium 7075-T6 (E_2 = 71 GPa and K_2 = 22 kN/mm) round bar with yield strength 430 MPa. The aluminium bar represented the spring in Fig. 1(a). Figure 4(b) illustrates two removable bars with length L_3' equal to 200 mm and diameter D_3' equal to 40 mm attached to the end of the plate in order to link the aluminium bar to the test machine frame. Again, all the fittings and connectors could introduce extra elastic follow-up into the specimen. The final elastic follow-up for this case is given by

$$Z = 1 + \frac{1}{\alpha} + \frac{1}{\beta} = 1 + \frac{K_1}{K_2} + \frac{K_1}{K_{CF}}, \tag{4}$$

where β is the stiffness ratio between the whole connectors/fittings and the test sample. The stiffness of the various connectors and fittings were determined in the same way as in Sec. II C. Using these values in Eq. (4) provided an elastic follow-up of 10.8 and this was sufficiently close to the target value of 10.5 to be acceptable.

E. Loading system

A stepper motor was used to apply a misfit (δ_0) that in turn introduced the load (σ_1) into the test machine, as illustrated in Figs. 1(a) and 4(c). The loading system included a stepper motor, a thrust ball bearing, two keyways, a worm gear and wheel, a linear shaft, and a coupling to link the motor to the worm gear [Fig. 4(c)]. A worm wheel was modified by manufacturing an M35 screw to fit the loading screw bar and a slot to include a thrust ball bearing. Two aluminium plates were made to fit the motor on the rig frame. Different loading strain rates were obtained by controlling the rotation speed of the stepper motor.

The holding torque T_h of the stepper motor was 12.1 N m, with a working temperature up to 90 °C.[32] The output torque decreased with an increase in the rotational speed of the motor and the torque reduced to about 8 N m at speeds of 180 rpm.[32] The rotational speed of the motor was always smaller than 180 rpm in the tests. Therefore, the output torque T_{op} of the

loading up system was calculated using

$$T_{op} = T_v \times \eta \times \psi = 122.5\ \text{N m}, \tag{5}$$

where T_v is the output torque of the stepper motor at a speed of v; η is the gear ratio between the worm wheel (4 starts) and the worm gear (68 teeth) which is 17; ψ is the gear transmission efficiency coefficient which is about 0.9 for 4 starts.

The total friction torque (T_f) exerted by the screw thread T_s and the thrust ball bearing with the raceway T_b can be calculated using

$$T_f = T_s + T_b = F \cdot \mu_s \cdot d + F \cdot \mu_b, \tag{6}$$

where F is the applied force and d is the nominal diameter of the screw. μ_s and μ_b are the dynamic and static friction coefficients, respectively. The dynamic friction coefficient of a bearing with the raceway and lubricant was assumed to be 0.09, and the static friction coefficient before the ball rotated was assumed to be 0.24.[33]

The motor can only rotate when the output torque of the loading system was larger than the total friction torque. Therefore, the maximum force that could apply using this system is 23.5 kN which was determined using $T_f = T_{op}$.

A stepper motor controller system was powered through a 220 voltage socket and a 10 m eternal cable was used to connect the controller system to a computer placed outside of the beam at the ENGIN-X instrument. The Labview software[34] was used to control the loading system.

F. Data acquisition

In addition to neutron spectra, the force, temperature, and strain or displacement were also monitored from the test machine during a test. The displacements in the test samples [bar 1 in Fig. 1(a)] were measured by using a modified axial extensometer, as shown in Fig. 5. The strain in the aluminium bar (bar 2) was measured by using three strain gauges located on the middle of the bar and placed 120° around the circumference of the bar. The specimen extensometer was made of Nimonic 80A. Two linear variable differential transformers (LVDTs) in the extensometer, with a stroke of ±2.5 mm, measured the sample extension with a displacement resolution of 2 μm at a maximum operating temperature of 80 °C.

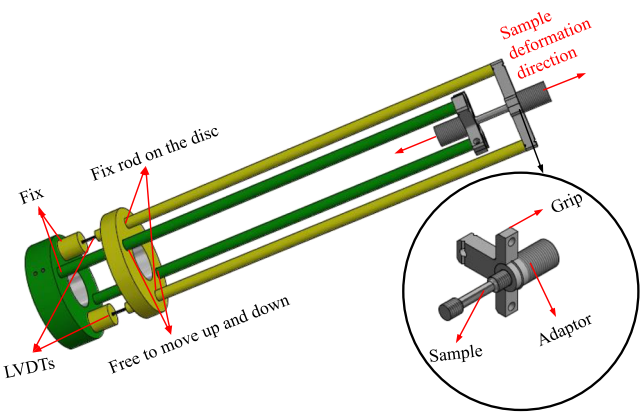

FIG. 5. A three-dimensional drawing to show an overview of the extensometry system.

The average of the voltages from the two LVDTs were used and considered to be the output value of the extensometer in accordance with BS EN 10291.[35] The temperature profile along the specimens was recorded using three K-type thermocouples attached to the top, mid, and bottom of the gauge length. A compact tension load cell was used to monitor the applied force.

The analog signals produced by three strain gauges, one load-cell, two LVDTs, and three thermocouples were recorded on a digital computer. A Vishay System 5000 data logger was used in conjunction with Vishay's "strain smart" data logging software (version 4.22). The entire apparatus was controlled by a custom graphical user interface (GUI) using Labview and National Instruments hardware. Only an external cable was required to connect to a computer to permit data acquisition and motor control.

III. EXPERIMENTAL PROCEDURE

There were several elements to the test procedure when using the new test machine in the ENGIN-X instrument. First, a sample and the extensometer had to be assembled into the test machine. The test machine and its sample were then lifted into the ENGIN-X beamline and mounted on the work table. This was followed by aligning the test machine and its sample in the neutron beam and the two detectors. Finally, high-temperature experiments using steel samples were conducted.

A. Specimen assembly

First, the extensometer was assembled on the specimen, followed by attaching three thermocouples to the top, middle, and bottom of the specimens. Four thermocouples were also placed on the two loading bars and the two outside bars to monitor temperatures at different positions of the test rig. The specimen was positioned in the centre of the furnace. The test machine with its specimen and extensometer, thermocouples, and load cell was then lifted into the beamline of the ENGIN-X instrument. It was ensured that the rods of the extensometer were positioned so that they did not interfere with the incoming and diffracted neutron beams.

B. Neutron beam alignment

A calibration was conducted to ensure that the neutron beam was directed at the centre of the test sample through the channel in the furnace, as shown in Figs. 2 and 3. An alignment was performed to ensure that the gauge volume was in the centre of the specimen. This was done by first introducing a laser beam that was coincident with the path of the neutron beam. Then the complete test machine and its sample were lifted onto the work table into the beamline. One half of the furnace was raised up, and a theodolite was used to make sure that the laser targeted the centre of the sample by adjusting the position of the work table. Good alignment was achieved when the laser beam was focused on the right side of the sample and there was no scattering of the laser beam.

Then the beamline was switched on and neutron spectra were obtained. The beamline was switched off and the furnace was closed, and the position of the furnace was adjusted to

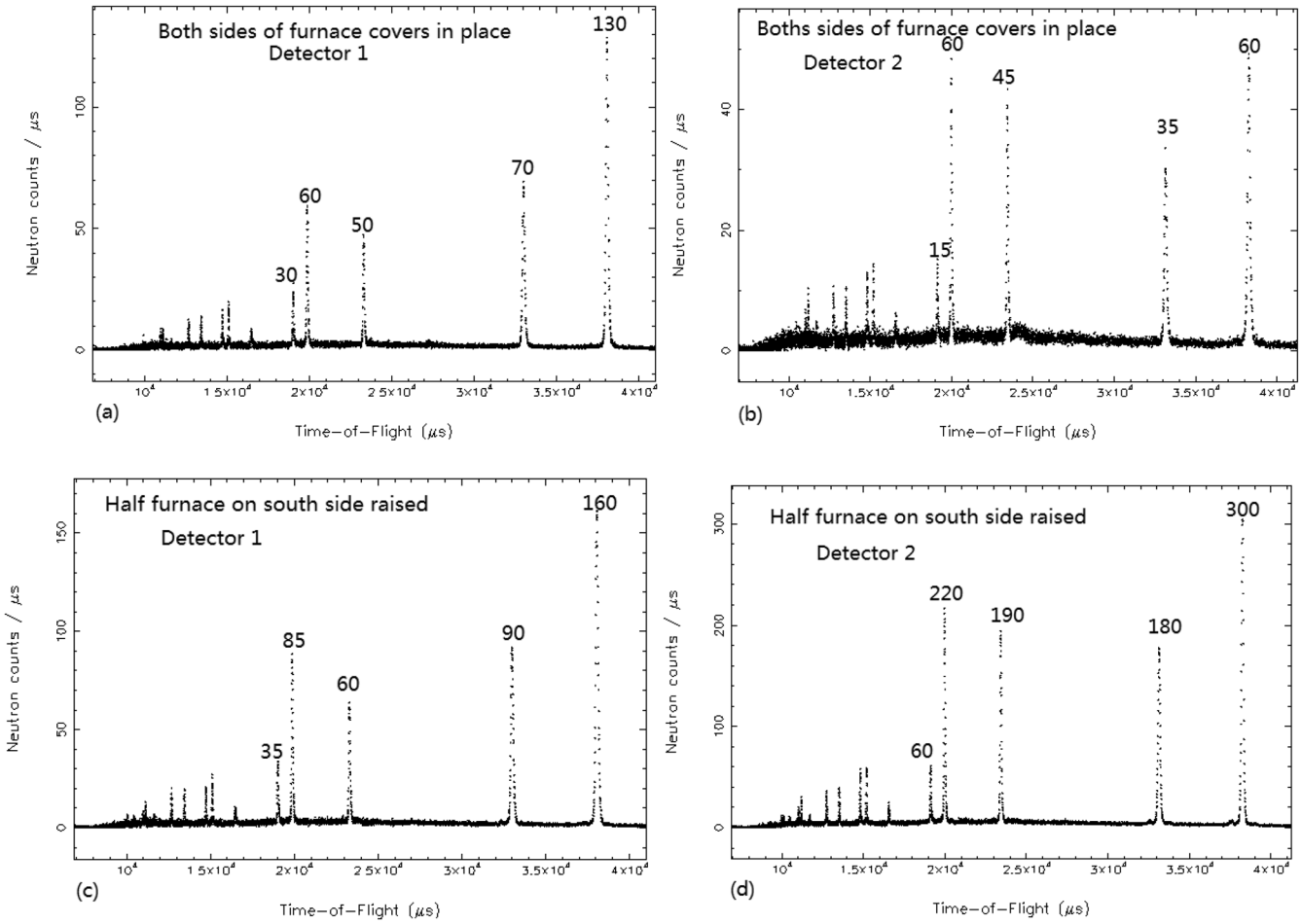

FIG. 6. Neutron spectra obtained during alignment of the experiment for two different cases. [(a) and (b)] Case 1, one half of the furnace is open; [(c) and (d)] Case 2, furnace covers are closed.

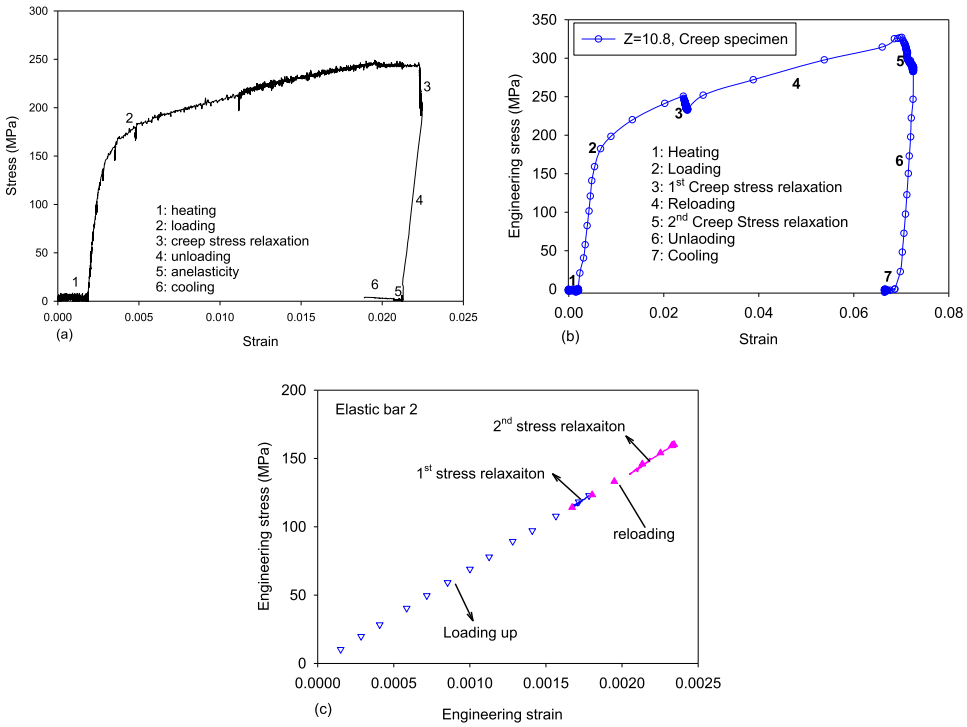

FIG. 7. Measured macrostress and strain for the test specimen with (a) Z ~ 1.2 and (b) Z ~ 10.5. Note that the different stages of the experiment are labelled; (c) the corresponding responses in the elastic bar 2 during 1st and 2nd loading up and stress relaxation stages, as shown in (b).

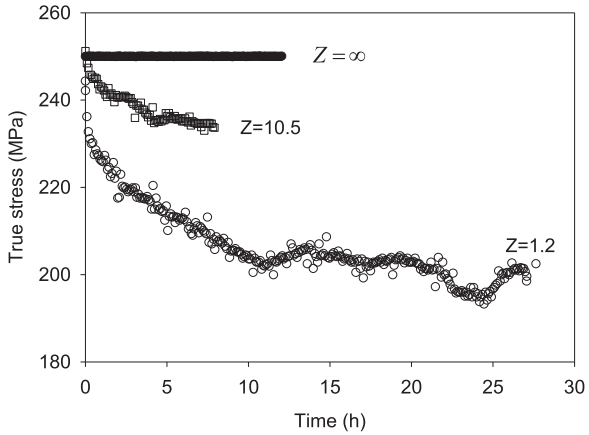

FIG. 8. The comparison of stress relaxation with similar initial applied stress (250 MPa) but different elastic follow-up factors infinitely large, ~10.5 and ~1.2.

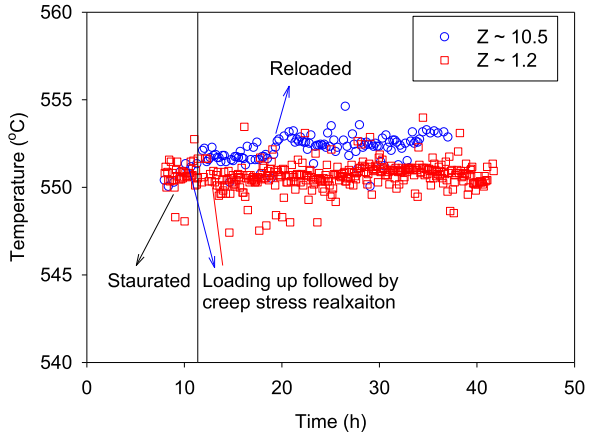

FIG. 9. Temperature profiles in the centre of samples during loading up and creep stress relaxation.

permit the laser beam to pass through the tube and target the sample. Then the beamline switched on and another neutron measurement conducted.

Figure 6 shows neutron spectra obtained from detectors 1 and 2 before [Figs. 6(a) and 6(b)] and after closing the furnace [Figs. 6(c) and 6(d)]. Note that detector 1 is the detector that is positioned with a ceramic section of the furnace removed, as illustrated in Fig. 3. Figures 6(a) and 6(c) show that the closure of the furnace did not modify the neutron spectra from detector 1.

The careful alignment of the test machine and its integral furnace in the ENGIN-X beamline ensured that during an experiment the axial intergranular strains of the metal test samples could be measured at high temperature. However, the system could only measure the neutron spectra from detector 1 and data from detector 2 were not used in the experiments. The experiments are described in Sec. III C.

C. High-temperature experiments

Experiments were conducted using an ex-service plus further laboratory aged type 316H austenitic stainless steel supplied by EDF energy.[26] Uniaxial samples were manufactured using this material, inserted into the new test machine and the test machine installed into the diffractometer, as explained earlier. Two samples were tested, one with Z ~ 1.2 and the other with Z ~ 10.5. In each case, the experimental procedure was the same. The test durations were relatively short (around several days) and were undertaken to demonstrate the capability of the test machine.

After ensuring that the alignment of the neutron beam with each specimen was complete, additional insulation was inserted into both ends of the furnace. The neutron beam was then switched on and arranged to ensure that each sample was illuminated with the beam so that there was a gauge volume of 4 × 4 × 4 mm for the diffraction measurements.

Each test specimen was first heated to 550 °C at a rate of 5 °C/min for a period of about 6 h and the system then soaked for 5 h to ensure that the test machine and the surrounding environment were at a stable temperature. During heating, diffraction data were obtained at 5 min intervals. The test sample was then loaded at a strain rate of 0.0067% s^{-1} and the stress in the gauge length was increased in 25 MPa steps until the target stress of 250 MPa was achieved. Again, diffraction data were obtained during loading with a measurement time of 10 min for each stress. The time to achieve maximum load was about 2 h. The stepper motor was then switched off once the target stress was achieved. The stress in the specimen then naturally decreased as elastic strain was converted to creep strain. Apart from controlling the specimen temperature, no additional external control of the test machine was required. For $Z = 10.5$, the specimen was reloaded to 350 MPa after 8 h relaxation from the initially applied stress of 256 MPa and further relaxed for about 13 h at 550 °C. Measurements of stress

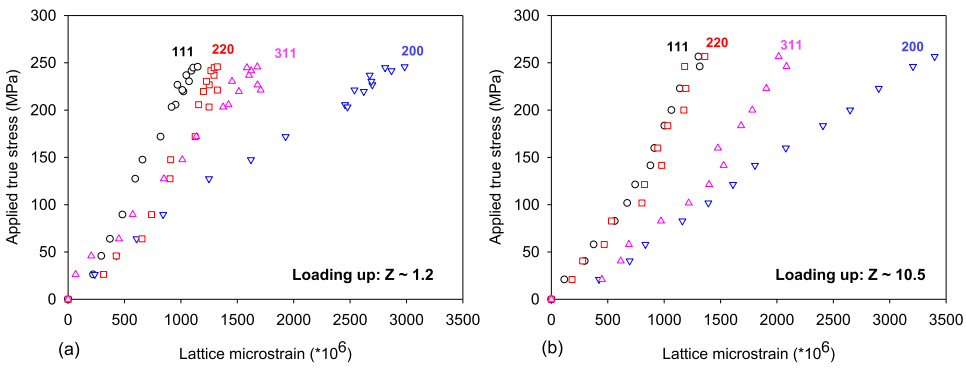

FIG. 10. Neutron diffraction measured elastic lattice strains along the axial direction of the Z ~ 1.2 (a) and Z ~ 10.5 (b) test specimens for 111, 200, 311, and 200 grain families during the loading stage.

relaxation lasted around 8-30 h, and diffraction measurements were made during stress relaxation.

IV. EXPERIMENTAL RESULTS AND DISCUSSION

The load cell, extensometer, and thermocouples in the test machine provided the macro stress, strain, and temperature of each test sample. Figures 7(a) and 7(b) illustrate the different stages of the macro-stress-strain behavior of the samples with Z ~ 1.2 and Z ~ 10.5 included heating, loading to the target stress, creep stress relaxation, unloading, and finally cool down phases. It can be seen in Figs. 7(a) and 7(b) that during loading to approximately 250 MPa the sample underwent elastic deformation and significant plastic deformation prior to creep stress relaxation. The measured elastic follow-up factor was obtained from the slopes of stress versus strain curves during the creep stress relaxation. It showed that the measured elastic follow-up factors were approximately 1.2, 10.5, and 10.8 (reloaded) which agreed excellently with the designed values. Figure 7(c) shows that the elastic aluminium bar acted like perfect elastic spring during both loading up and unloading. Figure 8 shows that the stress relaxation rate reduced as the elastic follow-up factor increased. The measured stresses were fluctuating slightly over time due to the fluctuations of room temperature. The stress relaxation curves agreed with the results obtained from laboratory experiments published in Ref. 6. The temperature profiles for both tests at the centre position of the samples during loading up and creep stress relaxation were very stable, as shown in Fig. 9. These results illustrated that this rig was able to provide accurate elastic follow-up factors, stable temperature profile, and mechanical responses.

TABLE I. Summary of derived diffraction elastic constants (DEC) from *in situ* neutron diffraction measurement at 550 °C, the materials are ex-service laboratory aged type 316H stainless steel. LC means the constant load control.

Test	E_{111} (GPa)	E_{200} (GPa)	E_{220} (GPa)	E_{311} (GPa)
Z ~ 1.2	185	101	160	125
Z ~ 10	170	87	144	118
LC	202	115	171	134
LC 2[18]	165	103	149	133
LC 3[18]	182	93	184	120
LC 4[37]	190	110	160	130

During each of the test stages, illustrated in Figs. 7(a) and 7(b), neutron diffraction data were analysed to obtain changes in crystal lattice spacing and then used to determine the internal lattice strains for each grain family. In the present work, four diffraction peaks (111, 200, 220, and 311) were considered. The strain for each orientation is given by

$$\varepsilon_{hkl} = \frac{d_{hkl} - d^0_{hkl}}{d^0_{hkl}}, \tag{7}$$

where ε_{hkl} is the elastic strain in the $\{hkl\}$ grain family, d_{hkl} and d^0_{hkl} are the stress and stress-free lattice spacings. The stress-free lattice spacing d^0_{hkl} for loading and stress relaxation was considered as the value when the sample was at 550 °C. Results presented here are confined only to loading and stress

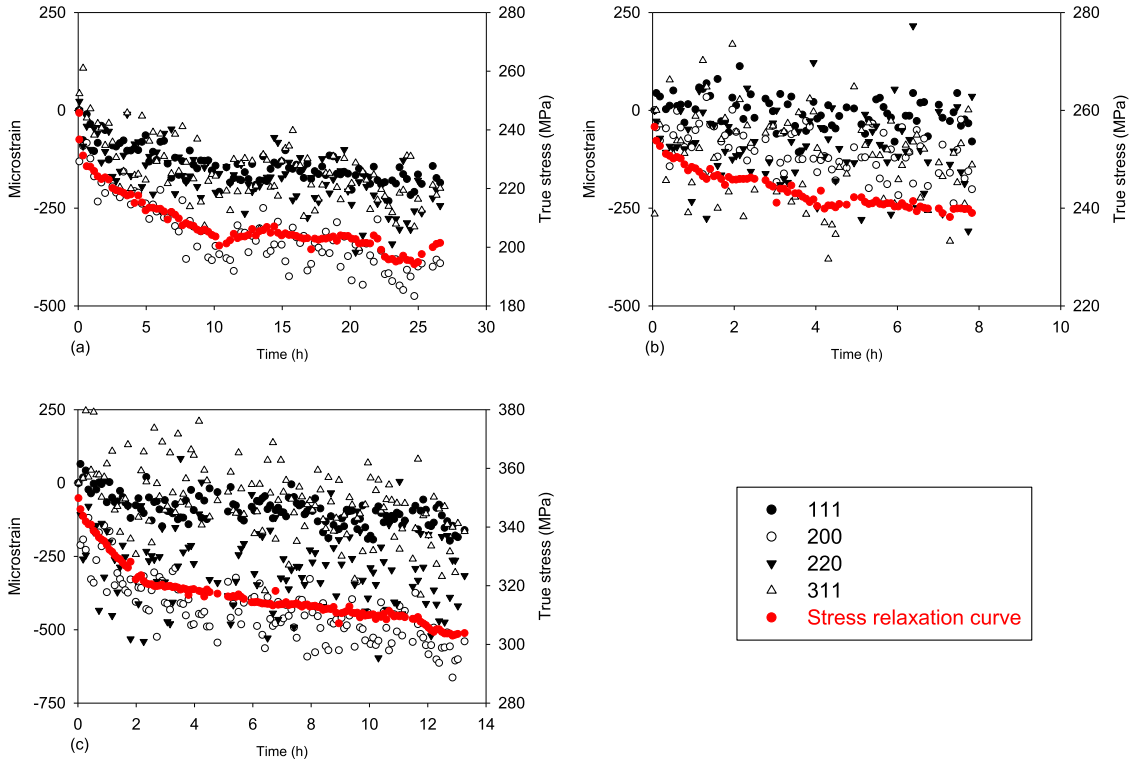

FIG. 11. Macrostress and lattice microstrain evolution measured *in situ* during the early stage of stress relaxation in type 316H austenitic stainless steel at 550 °C under (a) an initial applied stress of 250 MPa with Z ~ 1.2, (b) an initial applied stress of 250 MPa with Z ~ 10.5, and (c) a reloaded stress of 350 MPa with Z ~ 10.5.

relaxation. The typical uncertainties in the measured lattice strains were approximately ±30 microstrain.[18,36] However, the scatter of lattice strain measurements could be as larger as 200 microstrain, as shown in Refs. 17 and 26.

The evolution of lattice strains in grain families having 111, 200, 220, and 311 crystallographic planes aligned normal to the direction of loading during the loading stage for Z ~ 1.2 and 10.5 is shown in Figs. 10(a) and 10(b). The figure shows that the crystallographic planes deformed linearly to stresses lower than 125 MPa, which is similar to the macro-stress-strain response shown in Figs. 7(a) and 7(b). The diffraction elastic constants (DEC) for each lattice plane were obtained by using the ratio of applied stress to the lattice strains on each plane in the linear region. These constants derived from the loading up stage are summarized in Table I and are compared with the DEC obtained by using a hydraulic Instron tensile rig at ENGIN-X[18,37] with reasonable agreement. The initial elastic-plastic loading created misfit strains and stresses between the different crystallographic planes prior to stress relaxation.

The decreasing of the lattice strains on the 111, 200, 220, and 311 crystallographic planes for Z ~ 1.2 and 10.5 is shown in Figs. 11(a)–11(c). The lattice strains when samples were loaded to approximately 250 MPa were treated as zero. The greatest relaxation of lattice strains occurred for the 200 crystal plane and the least on the 111 crystal plane. However, as shown in Ref. 26, when the product of the relaxed lattice strain and the corresponding diffraction elastic constant were determined, it was found that stresses on the different crystal planes relaxed the same amount, and the trends in the relaxation of the lattice stresses agreed with the macroscopic stress relaxation. It should be noted that the DEC used in Ref. 26 were obtained from the unloading stage rather than the loading up stages presented in the current work. More scientific discussion about the results can be found in Ref. 26.

While the results were confined to short durations, the findings demonstrated that the new test rig has the potential for undertaking longer duration experiments. This would require the test machine being set up to operate continuously for several thousands of hours and moved periodically into the beamline for diffraction measurements. This is the subject of further research work.

V. CONCLUSIONS

A new test rig has been designed and commissioned to operate in the ENGIN-X instrument at the ISIS facility. The test rig was designed to allow test samples measured using neutron diffraction whilst being subjected to high temperatures and stress relaxation with the machine capable of subjecting samples to different levels of elastic follow-up. The test rig with its integral furnace was designed to be operated remotely away from the instrument beamline with only temperature control required.

A set of test samples were used to commission the test machine within the neutron beam environment. High-quality diffraction measurements from a sample of 316H austenitic stainless steel confirm that data of excellent intensity and resolution can be obtained from crystalline samples using the neutron diffraction technique. This apparatus will enable the study of creep behavior under constant load, constant strain, and elastic follow-up control for *in situ* tests at temperatures up to 800 °C with a maximum applied stress of 20 kN. The future work would test the feasibility of running long-term creep experiments at ENGIN-X using the current designed rig. The rig has to be mounted and un-mounted several times in the beamline to show the repeatability of the lattice strain measurement.

ACKNOWLEDGMENTS

This paper is dedicated to the memory of David Smith (1951-2015), Professor of Engineering Materials at the University of Bristol. This research was conducted with support from EDF-Energy and the ISIS facility. David Smith is supported by the Royal Academy of Engineering, EDF Energy and Rolls Royce plc. Mock-up setup and formal experiments were performed at the ENGIN-X, ISIS Pulsed Neutron Source with support by a beamtime (No. RB1310146) allocation from the Science and Technology Facilities Council.

APPENDIX: CALCULATION OF ELASTIC FOLLOW-UP IN A TWO-BAR MODEL

The total misfit (δ_0) in the two-bar model is equal to the displacement in bar 1 (specimen) added to the displacement in bar 2 (spring) during the creep under elastic follow-up control.[6] If we assume that creep deformation only takes place in the specimen, then the two bars followed a relationship of

$$\left(\varepsilon_{1-e}+\varepsilon_{1-p}+\varepsilon_{1-c}\right)L_1+\left(\varepsilon_{2-e}+\varepsilon_{2-p}\right)L_2=\delta_0, \tag{A1}$$

where ε_e, ε_p, ε_c, δ_0, and L represent the elastic strain, plastic strain, creep strain, total misfit, and length of bars, respectively. The subscripts 1 and 2 represent the specimen and bar 2, respectively. The elastic and plastic deformation in bars and total misfit (δ_0) are constant during creep. Therefore, differentiating Eq. (A1) gives

$$\dot{\varepsilon}_{1-e}L_1+\dot{\varepsilon}_{1-c}L_1+\dot{\varepsilon}_{2-e}L_2=0, \tag{A2}$$

where $\dot{\varepsilon}_{1-e}$ and $\dot{\varepsilon}_{1-c}$ are the elastic and creep strain rates in the specimen and $\dot{\varepsilon}_{2-e}$ is the elastic strain rate in bar 2.

Force equilibrium condition between two bars indicates that

$$\dot{\varepsilon}_{2-e}=\frac{A_1E_1L_2}{A_2E_2}\dot{\varepsilon}_{1-e}, \tag{A3}$$

where A and E represent the cross-sectional area and Young's modulus, respectively. By substituting Eq. (A3) into Eq. (A2), we obtain

$$\dot{\varepsilon}_{1-e}L_1\left(1+\frac{A_1E_1L_2}{A_2E_2L_1}\right)+\dot{\varepsilon}_{1-c}L_1=0, \tag{A4}$$

and rearranging

$$\dot{\varepsilon}_{1-e}=-\frac{1}{Z}\dot{\varepsilon}_{1-c}, \tag{A5}$$

where Z is the elastic follow-up factor in the two-bar model shown in Fig. 1(a) and can be described as

$$Z=1+\frac{A_1E_1L_2}{A_2E_2L_1}=1+K_2/K_1=1+1/\alpha, \tag{A6}$$

where α is the stiffness ratio between the specimen (K_1) and the bar 2 (K_2).

The elastic strain in the specimen is given by

$$\dot{\varepsilon}_{1-e} = \frac{\sigma_1}{E}. \tag{A7}$$

Substituting Eq. (A7) into Eq. (A5), we obtain

$$\dot{\sigma}_1 = -\frac{1}{Z} E_1 \dot{\varepsilon}_{1-c}, \tag{A8}$$

where $\dot{\sigma}_1$ is the stress relaxation rate in the specimen, $\dot{\varepsilon}_{1-c}$ is the creep strain rate in the specimen which can be described by any constant-load creep model. According to Eq. (A8), the stress in the specimen will reduce as the elastic strain is replaced by creep strain. The total strain rate in the specimen during creep can be obtained by adding the elastic strain rate to the creep strain rate, giving

$$\dot{\varepsilon}_1 = \dot{\varepsilon}_{1-e} + \dot{\varepsilon}_{1-c} = (1 - Z)\frac{\dot{\sigma}_1}{E_1}. \tag{A9}$$

Equation (A9) can also be rearranged to

$$Z = 1 - \frac{\Delta\varepsilon_1 E_1}{\Delta\sigma_1} = 1 + \frac{\Delta\varepsilon_1 E_1}{|\Delta\sigma_1|}, \tag{A10}$$

where $\Delta\sigma_1$ and $\Delta\varepsilon_1$ are the relaxed stress and accumulated strain in the specimen during creep stress relaxation.

The elastic follow-up factor in the two-bar model can be predicted by using Eq. (A6) or measured from the stress-strain curve trajectory [Eq. (A10)].

[1] E. L. Robinson, "The resistance to relaxation of materials at high temperature," Trans. ASME **61**, 543–554 (1939).
[2] R. A. Ainsworth, R5: Assessment procedure for the high temperature response of structures, Vol. 3, British Energy Generation Ltd., 2003.
[3] RCC-MR, Design and Construction Rules For Mechanical Components of FBR Nuclear Islands, Section 1, Sub-sections Z, Technical Appendix A3, AFCEN, 1985.
[4] ASME Boiler and Pressure Vessel Code, Section III-Rules for Construction of Nuclear Power Plant Components, Vol. 2, 1992.
[5] Y. Q. Wang, D. J. Smith, and C. E. Truman, "Inelastic deformation and elastic follow-up," in *ASME 2013 Pressure Vessels and Piping Conference* (American Society of Mechanical Engineers, 2013).
[6] Y. Wang, H. Coules, C. Truman, and D. Smith, "Effect of elastic follow-up and ageing on the creep of an austenitic stainless steel," Int. J. Solids Struct. **135**, 219–232 (2018).
[7] Y. Q. Wang, M. W. Spindler, C. E. Truman, and D. J. Smith, "Critical analysis of the prediction of stress relaxation from forward creep of type 316H austenitic stainless steel," Mater. Des. **95**, 656–668 (2016).
[8] K.-H. Lee, Y.-J. Kim, D. W. Jerng, R. A. Ainsworth, and D. Dean, "Creep elastic follow-up factors under multi-axial displacement-controlled loading," Int. J. Mech. Sci. **57**(1), 54–62 (2012).
[9] J. T. Boyle, "Stress relaxation and elastic follow-up using a stress range-dependent constitutive model," Proc. Inst. Mech. Eng., Part C **226**(6), 1472–1483 (2012).
[10] K. Kobayashi, S. Abe, and T. Udoguchi, "Stress and strain behaviors under uniaxial elastic follow-up," Bull. JSME **29**(257), 3672–3678 (1986).
[11] K. Kobayashi, Y. Saitoh, and T. Udoguchi, "Estimation of elastic follow-up behavior on 18Cr-8Ni steel using simplified inelastic analysis," J. Pressure Vessel Technol. **116**(2), 136–140 (1994).
[12] K. Naoto, N. Takashi, I. Koji, and N. Hitoshi, "Advanced creep-fatigue evaluation rule for fast breeder reactor components: Generalization of elastic follow-up model," Nucl. Eng. Des. **155**(3), 499–518 (1995).
[13] K. Kobatake, H. Ohta, H. Ishiyama, T. Kaihara, and O. Ueno, "An alternate approach to creep-fatigue damage with elastic follow-up for high temperature structural design," J. Natl. Fish. Univ. **48**(1), 25–39 (1999).
[14] N. Isobe, S. Sakurai, M. Yorikawa, K. Imou, and Y. Takahashi, "Life prediction of 316FR stainless steel under creep–fatigue loading with elastic follow-up," Int. J. Pressure Vessels Piping **77**(13), 817–823 (2000).
[15] Y. Q. Wang, "Design, development and experiments to investigate the effect of elastic follow-up on creep stress relaxation in austenitic steels," Ph.D. thesis, Department of Mechanical Engineering, University of Bristol, UK, 2015.
[16] A. Rao, K. B. Chong, P. J. Bouchard, and M. E. Fitzpatrick, "Internal stress generation in austentic stainless steels during creep deformation," in *ASME 2011 Pressure Vessels and Piping Conference* (American Society of Mechanical Engineers, 2011), pp. 215–225.
[17] A. Rao, P. J. Bouchard, S. M. Northover, and M. E. Fitzpatrick, "Anelasticity in austenitic stainless steel," Acta Mater. **60**(19), 6851–6861 (2012).
[18] B. Chen, J. N. Hu, P. E. J. Flewitt, D. J. Smith, A. C. F. Cocks, and S. Y. Zhang, "Quantifying internal stress and internal resistance associated with thermal ageing and creep in a polycrystalline material," Acta Mater. **67**, 207–219 (2014).
[19] B. Chen, P. E. J. Flewitt, A. C. F. Cocks, and D. J. Smith, "A review of the changes of internal state related to high temperature creep of polycrystalline metals and alloys," Int. Mater. Rev. **60**(1), 1–29 (2014).
[20] B. Chen, J. N. Hu, Y. Q. Wang, S. Y. Zhang, S. Van Petegem, A. C. F. Cocks, D. J. Smith, and P. E. J. Flewitt, "Role of the misfit stress between grains in the Bauschinger effect for a polycrystalline material," Acta Mater. **85**, 229–242 (2015).
[21] J. N. Hu and A. C. F. Cocks, "Effect of creep on the Bauschinger effect in a polycrystalline austenitic stainless steel," Scr. Mater. **128**, 100–104 (2017).
[22] E. Oliver, J. Santisteban, J. James, M. Daymond, and J. Dann, ENGIN-X User Manual, ISIS, Rutherford Laboratory, Didcot, UK, 2004.
[23] R. Woracek, D. Penumadu, N. Kardjilov, A. Hilger, M. Strobl, R. C. Wimpory, I. Manke, and J. Banhart, "Neutron Bragg-edge-imaging for strain mapping under *in situ* tensile loading," J. Appl. Phys. **109**(9), 093506 (2011).
[24] H. M. Reiche, S. C. Vogel, P. Mosbrucker, E. J. Larson, and M. R. Daymond, "A furnace with rotating load frame for *in situ* high temperature deformation and creep experiments in a neutron diffraction beam line," Rev. Sci. Instrum. **83**(5), 053901 (2012).
[25] H. A. Bale, A. Haboub, A. A. MacDowell, J. R. Nasiatka, D. Y. Parkinson, B. N. Cox, D. B. Marshall, and R. O. Ritchie, "Real-time quantitative imaging of failure events in materials under load at temperatures above 1,600 °C," Nat. Mater. **12**(1), 40–46 (2013).
[26] Y. Q. Wang, S. Hossain, S. Kabra, S. Zhang, D. Smith, and C. Truman, "Effect of boundary conditions on the evolution of lattice strains in a polycrystalline austenitic stainless steel," J. Mater. Sci. **52**(13), 7929–7936 (2017).
[27] W. Kuhs, J. Archer, and D. Doran, "A closed-shell furnace for neutron single-crystal diffraction," J. Appl. Crystallogr. **26**(5), 730–733 (1993).
[28] F. P. Bailey and C. E. G. Bennett, "A simple furnace for neutron diffraction studies," J. Appl. Crystallogr. **12**(4), 403–404 (1979).
[29] S. J. Moorhouse, N. Vranjes, A. Jupe, M. Drakopoulos, and D. OHare, "The Oxford-diamond *in situ* cell for studying chemical reactions using time-resolved x-ray diffraction," Rev. Sci. Instrum. **83**(8), 084101-1–084101-8 (2012).
[30] M. Yashima, "*In situ* observations of phase transition using high-temperature neutron and synchrotron x-ray powder diffractometry," J. Am. Ceram. Soc. **85**(12), 2925–2930 (2004).
[31] J. Santisteban, M. Daymond, J. James, and L. Edwards, "ENGIN-X: A third-generation neutron strain scanner," J. Appl. Crystallogr. **39**(6), 812–825 (2006).
[32] Stepper Motors and Encoders, National Instruments, 2014.
[33] G. Pahl, W. Beitz, K. Wallace, and D. Council, *Engineering Design* (Springer, 1984).
[34] LabVIEW User Manual, National Instruments, Austin, TX, 1998.
[35] British Standards Institute, Metallic Materials—Uniaxial Creep Testing in Tension—Method of Test, BS EN 10291:2000, London, 2000.
[36] B. Cai, B. Liu, S. Kabra, Y. Wang, K. Yan, P. D. Lee, and Y. Liu, "Deformation mechanisms of Mo alloyed FeCoCrNi high entropy alloy: *In situ* neutron diffraction," Acta Mater. **127**, 471–480 (2017).
[37] M. R. Daymond and P. J. Bouchard, "Elastoplastic deformation of 316 stainless steel under tensile loading at elevated temperatures," Metall. Mater. Trans. A **37**(6), 1863–1873 (2006).